Optimal design of wind machine impeller for frost protection based on CFD and its field test on airflow disturbance

Wu Wenye[1], Hu Yongguang[1*], Yang Shuo[1], Mao Kangqian[1], Zhu Xiaoyong[1], Li Pingping[2]

(1. *School of Agricultural Equipment Engineering, Jiangsu University, Zhenjiang 212013, China*;
2. *College of Biology and the Environment, Nanjing Forestry University, Nanjing 210037, China*)

Abstract: Wind machines have been increasingly applied to prevent frost damage through airflow disturbance in tea fields and orchards. An impeller is the most important component of the machine. However, there are few studies on customized impeller design or airflow disturbance performance. The objective of this study was to design a new impeller for frost protection wind machines based on reverse engineering and CFD simulation. The characteristic parameters of an impeller include blade cross-section shape, installation angle, sweep angle, hub ratio and blade number. The optimal combination of the above parameters was obtained through the simulation of the impeller's aerodynamic performance. Field tests were conducted in a tea field to evaluate airflow disturbance performance of the designed impeller. The result shows that at a certain rotation speed and rotation diameter, the optimal combination of impeller parameters was: single arc cross-section of ϕ2400 mm, installation angle of 15°, sweep angle of 87°, hub ratio of 0.3 and blade number of 4, of which the impeller could achieve the highest usage of 0.56, the least consumed power of 1.363 kW and more uniform distribution of surface pressure on the windward side. Compared with other commercial frost protection wind machines, the maximum airflow velocity of the developed impeller was higher at 12 m in front of it. The probability of airflow velocity above 3.0 m/s within 30 min was the highest (71.7%), indicating its improvement of airflow stability. Without swing the new impeller could cover an effective area of 300 m^2, which was similar to that of the commercial ones.

Keywords: frost protection, wind machine impeller, CFD, reverse engineering, airflow disturbance, tea orchard
DOI: 10.3965/j.ijabe.20150805.1415

Citation: Wu W Y, Hu Y G, Yang S, Mao K Q, Zhu X Y, Li P P. Optimal design of wind machine impeller for frost protection based on CFD and its field test on airflow disturbance. Int J Agric & Biol Eng, 2015; 8(5): 43－49.

1 Introduction

Frosts might bring about serious cold injury to thermophilic crops and cause sizable loss to the production. The crops are easily suffered from late spring cold usually followed by frost events, since the buds are sprouting with high water content[1-4]. Radiation frost is more common in subtropical and temperate region during calm and clear nights. It occurs when a net energy loses through radiation from the earth surface to the sky, forming a thermal inversion layer near the ground, and temperature increases with height. It is necessary to break the vertical stratification of temperature to block the decrease of temperature near the ground[5-7]. Therefore, wind machines have been applied for frost protection by pushing warmer air aloft downwards to the canopies, or drawing and discharging cold air on the bottom upwards to the top of the layer or out of the protected area[8-11].

Received date: 2014-09-18 **Accepted date:** 2015-09-29
Biographies: Wu Wenye, Master student, Research interest: agricultural mechanization, Email: wwyzhshsh0308@163.com; **Yang Shuo**, Master student, Research interest: agricultural frost protection, Email: 470493337@qq.com; **Mao Kangqian**, Master student, Research interest: agricultural machinery, Email: maokangqian@163.com; **Zhu Xiaoyong**, PhD, Professor, Research interest: design on permanent magnet motor, Email: zxyff@ujs.edu.cn; **Li Pingping**, PhD, Professor, Research interest: agro-biological environment, Email: lipingping@ujs.edu.cn.
***Corresponding author: Hu Yongguang**, PhD, Professor, Research interest: agro-biological environmental engineering, monitoring and control of frost protection. Address: 301 Xuefu Road, Zhenjiang 212013, China. Tel: +86-511-88797338, Email: deerhu@ujs.edu.cn.

An impeller is the most important component of the machine, and its blade decides the protection effect of wind machines. So far there are two types of main blades used for frost protection wind machines. One is airfoil blade and the other is circular-plate blade[12,13]. The airfoil-blade impeller is similar to a helicopter rotor and widely used for large wind machines in USA, and its airfoil is concave-convex. Its rotation diameter varies from 3.0 m to 6.0 m and it is installed on the top of a pillar of 8-10 m tall. This type of wind machine is commercially available from some manufacturing companies, such as Orchard-Rite, Amarillo, Hauff and Vamco[14-16]. The machines are used for frost protection mainly in vineyards and orchards with the protected area of 2-4 hm^2. Yang[17] adopted a biconvex-airfoil blade and developed an impeller for a frost protection wind machine. Its rotation diameter was 4.44 m and the depression angle of the impeller was 14°. Wu et al.[16] carried on an airfoil optimization design based on Profili software and orthogonal test. Lift coefficient of the optimal airfoil increased by 15.48% and lift-drag ratio increased by 8.34% at 5° angle of attack, and stall performance of the airfoil was improved as well. The innovation of airfoil blade design has improved airflow disturbance performance and promoted the industry of large wind machines for frost protection.

On the other hand, the circular-plate blade is usually adopted to develop a type of small wind machine (called anti-frost fan in Japan) for tea plants[18,19]. The rotation diameter of its 3-blade impeller is 0.6-1.26 m and the installation height is 5.8-7.5 m. It could cover the protected area of 800-1000 m^2 with a large amount of airflow volume of 1000-6000 m^3/min. Some companies such as Fulta, Navec, and Sowa Technica provide growers with all types of wind machines. Qian et al.[20,21] analyzed the vibration and stress of the fans for low-noise strength design. Hu et al.[18,22] designed the first 4-blade wind machine in China for tea and developed a controller based on critical temperature and thermal inversion strength. Its protected area was about 900 m^2. However, few studies are involved with customized impeller design and analysis on its airflow disturbance performance.

The objective of this work is to design a new impeller for frost protection wind machines. And field tests were conducted to evaluate its airflow disturbance performance with the developed impeller.

2 Impeller simulation design

2.1 Design method

The impeller usually has a complex shape and curved surface, and there are many factors influencing its airflow disturbance performance, such as rotation speed, blade number, impeller diameter, installation angle, blade section shape, sweep angle and hub ratio[23]. To design an optimal customized impeller, a commercial base impeller was selected to obtain its characteristic parameters through model reconstruction based on reverse engineering. The reconstruction was done through Imageware (Siemens, Germany) and Pro/E (PTC, USA) to acquire the parameters' value.

The aerodynamic simulation in a hypothetical wind tunnel under different levels of the parameters was done to select the optimal parameters' combination[24,25]. Gambit and Fluent (ANSYS, USA) was used to generate model grids and CFD simulation. The post-processing tool (Tecplot, USA) was used to illustrate the simulation results.

2.2 Base impeller reconstruction

Reverse engineering is a technology of establishing digital models from a product prototype with complex surfaces. It has become an effective tool of new product design and development. Its basic step includes measurement of model surface, point cloud pretreatment, surface model reconstruction, and digital model export[26,27].

A 3-D laser scanner INFINITE 2.0-5124 (Hexagon Metrology, USA) was employed to scan the NK-1028YD blades (Navec, Japan) from different angles and directions. After the pretreatment of data smoothing, filtering compression and the like, the point clouds were exported as Iges-format file. The point clouds are shown in Figure 1, which was input to Imageware for model reconstruction. The feature of contour curve was extracted to form the impeller's edge profile by fitting the point clouds on the edge. Then as many as

section-curves on the point clouds were fit and smoothed, and spread into the blade surface after mending, cutting and seaming. Finally, the entity model was built via lofting, sweeping and arraying with Pro/E, shown in Figure 2. Characteristic parameters of the base impeller are listed in Table 1.

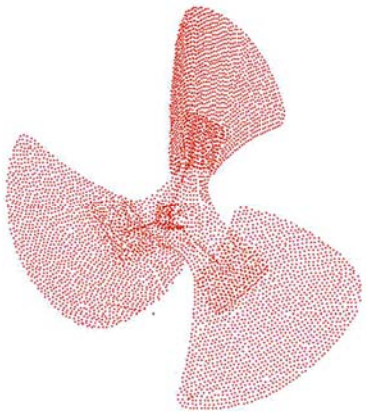

Figure 1 Scanned point cloud of the base impeller

Figure 2 3-D entity model of the base impeller

Table 1 Characteristic parameters of the base impeller

Installation angle/(°)	Sweep forward angle/(°)	Hub ratio	Blade number	Diameter of cross-section arc/mm
18	86	0.25	3	2 200

2.3 Aerodynamic simulation

2.3.1 Control equation

The airflow on the impeller was incompressible over time with a subsonic velocity, and there was no energy transfer. Thus, the continuity equation and the momentum equation were applied to the simulation.

Continuity equation:

$$\frac{\partial \rho}{\partial t}+\frac{\partial(\rho u_x)}{\partial x}+\frac{\partial(\rho u_y)}{\partial y}+\frac{\partial(\rho u_z)}{\partial z}=0 \quad (1)$$

where, u_x, u_y, u_z are velocity vectors, m/s; t is time, s; ρ is air density, kg/m^3.

Momentum equation:

$$\frac{\partial(\rho u_x)}{\partial t}+\nabla\cdot(\rho u_x\vec{u})=-\frac{\partial p}{\partial x}+\frac{\partial \tau_{xx}}{\partial x}+\frac{\partial \tau_{yx}}{\partial y}+\frac{\partial \tau_{zx}}{\partial z}+\rho f_x \quad (2)$$

$$\frac{\partial(\rho u_y)}{\partial t}+\nabla\cdot(\rho u_y\vec{u})=-\frac{\partial p}{\partial x}+\frac{\partial \tau_{xy}}{\partial x}+\frac{\partial \tau_{yy}}{\partial y}+\frac{\partial \tau_{zy}}{\partial z}+\rho f_y \quad (3)$$

$$\frac{\partial(\rho u_z)}{\partial t}+\nabla\cdot(\rho u_z\vec{u})=-\frac{\partial p}{\partial x}+\frac{\partial \tau_{xz}}{\partial x}+\frac{\partial \tau_{yz}}{\partial y}+\frac{\partial \tau_{zz}}{\partial z}+\rho f_z \quad (4)$$

where, p is intensity of pressure, Pa; τ is viscous stress vector, Pa; f_x, f_y, f_z are mass forces, m/s^2.

2.3.2 Entity model and grid generation

As shown in Figure 3, a hypothetical wind tunnel (ϕ2.0 m×30.0 m) was established to conduct CFD simulation under different combinations of the impeller parameters. The impeller was placed vertical to the longitudinal axis of the tunnel with its distance of 10.0 m to the inlet. When rotated at a given speed, the impeller pushed air by thrust-pressure. The grids of the entity model were generated with Gambit. The impeller and rotation region were specified as elements of pyramid, and the tunnel were specified as hex/wedge elements. The total cells were 301 337.

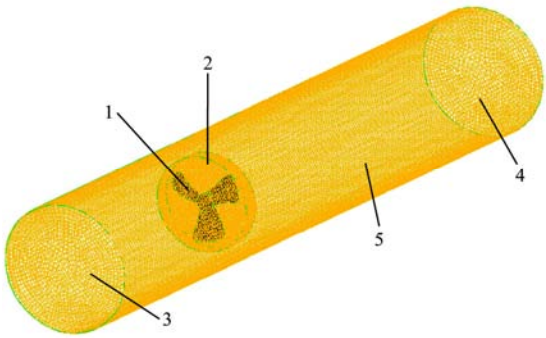

1. Impeller 2. Rotation region 3. Inlet 4. Outlet 5. Wind tunnel

Figure 3 Grid generation of the entity model

2.3.3 Boundary condition and solver selection

The boundaries of the impeller, inlet, outlet, rotation region and the tunnel surface were defined as follows: the impeller as the wall, inlet as pressure-inlet, outlet as pressure-outlet. The interface between the tunnel and rotation region was specified as interior boundary.

The energy equation was ignored and the solver was pressure and implicit formulation-based. And the k-ε standard model was selected as calculation model. The flow and turbulence solution were based on second-order upwind and SIMPLE algorithm.

2.4 Simulation results and analysis

2.4.1 Univariate simulation

As factors, blade cross-section shape, installation angle, sweep angle, hub ratio and blade number have

their unique influence on the aerodynamic indexes of airflow volume, velocity, consumed power and usage value. The aerodynamic performance simulation was done for each factor when the other factors are constant. The univariate simulation results are as follows.

(1) With the increase of installation angle, air volume and consumed power increased significantly, while usage value decreased. When the angle was above 30°, the stall phenomenon occurred. Within 15-20°, the indexes were acceptable. (2) The cross-sections of circular plate were superior to flat ones. The single arc (ϕ2200-2400 mm) and biarc (ϕ1600 mm and ϕ5000 mm) were selected for the following optimal simulation. (3) To a certain extent, airflow volume, total pressure and usage value increased with sweep angle, but too large angle would reduce usage value and require higher strength for blade materials. Forward and backward sweep angles of 87° and −87° were favorable. (4) Too large hub ratio sharply reduced usage value and if it was too small, the stall would occur, also causing low usage value. Taking aerodynamic performance, stiffness and strength of the impeller into account, hub ratio range should be 0.30-0.32.

2.4.2 Selection of the optimal impeller

Given the impeller rotation diameter of 1.0 m and rotation speed of 960 r/min, 24 treatments were arranged with different combinations of the parameters and then were simulated to investigate the aerodynamic indexes. With the limit of consumed power below 3.0 kW, the optimal impellers were selected as the ones corresponding to Treatment No.9, 10, 17 and 18 in Table 2.

Table 2 The results of the orthogonal test

Treatments	Installation angle /(°)	Cross-section	Sweep angle /(°)	Hub ratio	Blade number	Airflow volume /$m^3 \cdot s^{-1}$	Total pressure /Pa	Consumed power /W	Usage value
1	15	Arc ϕ2200	87	0.30	3	22.7	52.8	1199	0.61
2	16	Arc ϕ2200	87	0.32	4	25.3	66.0	1669	0.48
3	18	Arc ϕ2200	-87	0.32	3	26.6	70.7	1880	0.44
4	20	Arc ϕ2200	-87	0.30	4	28.3	82.4	2329	0.38
5	15	Arc ϕ2200	-87	0.32	4	21.9	94.4	2065	0.36
6	16	Arc ϕ2200	-87	0.32	3	24.3	60.5	1469	0.51
7	18	Arc ϕ2200	87	0.32	4	25.9	69.8	1805	0.45
8	20	Arc ϕ2200	87	0.32	3	25.5	66.1	1682	0.49
9	15	Arc ϕ2400	87	0.30	4	23.6	57.7	1363	0.56
10	16	Arc ϕ2400	87	0.32	3	23.8	57.2	1359	0.56
11	18	Arc ϕ2400	-87	0.32	4	27.4	76.7	2099	0.40
12	20	Arc ϕ2400	-87	0.30	3	26.5	70.4	1863	0.44
13	15	Arc ϕ2400	-87	0.32	3	24.2	58.3	1409	0.53
14	16	Arc ϕ2400	-87	0.32	4	25.3	65.4	1655	0.48
15	18	Arc ϕ2400	87	0.32	3	24.2	60.0	1451	0.52
16	20	Arc ϕ2400	87	0.32	4	27.8	79.9	2216	0.40
17	15	Biarc	87	0.30	4	23.8	58.9	1400	0.55
18	16	Biarc	87	0.32	3	24.0	58.9	1411	0.55
19	18	Biarc	-87	0.32	4	27.8	79.7	2217	0.39
20	20	Biarc	-87	0.30	3	26.6	71.6	1903	0.44
21	15	Biarc	-87	0.32	3	24.5	60.5	1481	0.52
22	16	Biarc	-87	0.32	4	25.5	66.8	1702	0.47
23	18	Biarc	87	0.32	3	24.2	60.7	1471	0.52
24	20	Biarc	87	0.32	4	28.0	82.6	2314	0.40

Furthermore, the distribution of surface pressure on the windward side is shown in Figure 4. For the impellers of Treatments No.9 and 10, the distribution was more uniform with smooth transition of the pressure. The airflow volume-efficiency plot in Figure 5 shows that the efficiency of Treatment No.9 was higher than that of Treatment No.10. Therefore, the impeller of Treatments No.9 was selected as the final design model, and its

characteristic parameters are listed in Table 3. The impeller could achieve usage value of 0.56 with consumed power of only 1.363 kW.

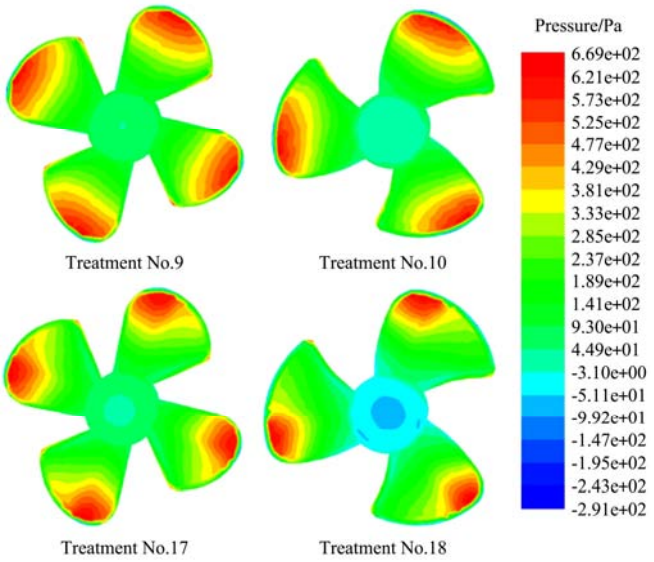

Figure 4 Distribution of surface pressure on the windward side

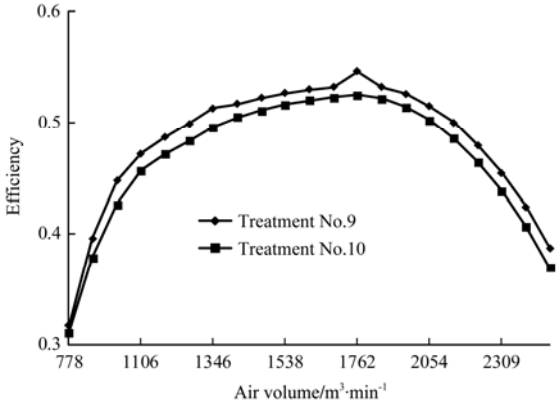

Figure 5 Airflow volume-efficiency curve

Table 3 Characteristic parameters of the optimal impeller

Installation angle/(°)	Sweep forward angle/(°)	Hub ratio	Blade number	Diameter of cross-section arc/mm
15	87	0.3	4	2400

3 Field test of airflow disturbance performance

3.1 Materials and methods

Field tests were conducted on Maichun tea plantation in Danyan, Jiangsu Province (Latitude 32°01′35″N, Longitude 119°40′21″E, Altitude 17 m). The wind machine impellers of the developed, Fulta and Navec were used for test. The specifications are shown in Table 4. Measurement instrumentations included a portable anemometer NK4000 (Kestrel, USA), a GIS collector XH6000 (Trimble, USA) and a sound-level meter AWA5680 (Aihua, China).

Under no wind or breeze conditions, the wind machines were started to disturb airflow above the tea fields. Airflow velocity around tea canopies was measured in a rectangular block (36 m×30 m) in front of the machines. One hundred and thirty-two anemometers were set at the top of the canopies with a spacing of 3.0 m between two adjacent anemometers (Figure 6). Due to the instantaneity and turbulence of the airflow, the maximum of five measurements was recorded. Another 60 measurements were collected at 12 m in front the machines every 30 s, with which the times of every velocity interval were counted. The boundary of an area was positioned with the GIS collector, where the velocity was above 0.6 m/s, and its area was calculated through GISoffice (Trimble, USA). The noise was measured at 12 m in front of the machines.

Table 4 Basic parameters of wind machines

Wind machines	Number of blades	Mounting height/m	Blade weight /kg	Diameter /mm	Angle of depression /(°)	Rotation speed /r·min^{-1}
Fulta	3	6.8	7.3	1000	47	960
Navec	3	7.1	8.3	1000	47	960
The developed	4	7.1	11.1	1100	47	960

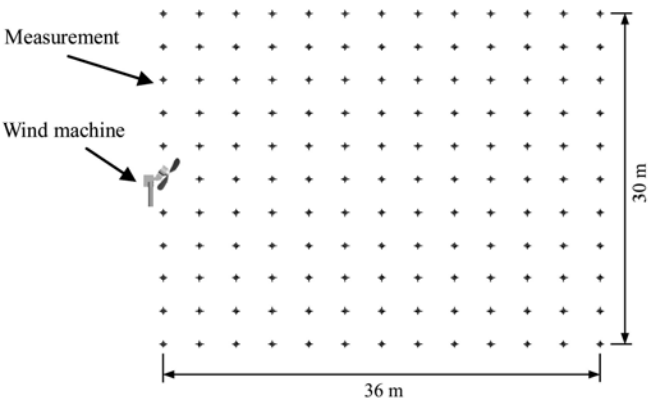

Figure 6 Layout of airflow velocity measurements

3.2 Results and analysis

3.2.1 Variation of airflow velocity

Figure 7 shows the airflow velocity variation within 33 m in front of the wind machines. The velocity decreased with the distance from the machines. Each machine had a dead zone within 6 m from it, where there was no airflow. The developed impeller could maintain airflow velocity above 2.0 m/s from 9 m to 27 m in front of it, and the velocity gradually dropped below 1.0 m/s beyond 30 m away. The highest airflow velocity of the

developed impeller was 4.8 m/s, higher than those of the Fulta and Navec impellers, which were 4.4 m/s and 4.0 m/s, respectively.

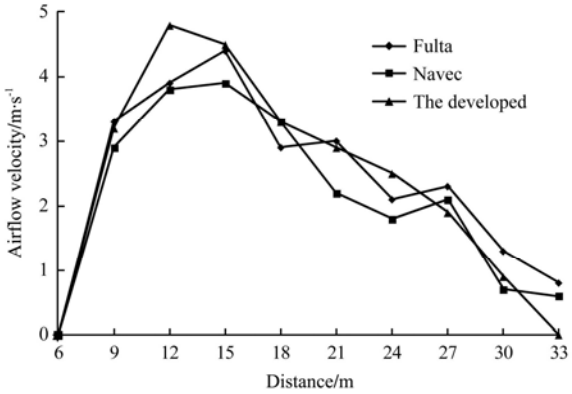

Figure 7 Airflow velocity in front of the wind machine

3.2.2 Stability of disturbed airflow

Figure 8 is the times of every velocity interval for the three impellers. After the statistical calculation of the 60-time measurement, the probability values of airflow velocity above 3.0 m/s were 71.7%, 61.7% and 56.4% for the developed, Fulta and Navec impellers, respectively. As for the developed impeller, its probability of airflow velocity above 3.5 m/s was the highest. Thus, the impeller of the developed machine improved the stability of disturbed airflow.

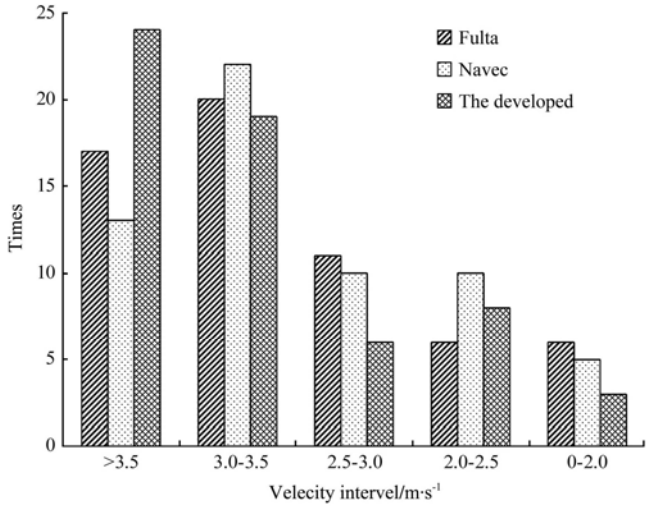

Figure 8 The times of every velocity interval

3.2.3 Analysis on other performance

It was found that airflow velocity at a distance of 30 m was very low for all the impellers (Table 5), and the velocity of 0.6 m/s is usually the lowest for effective frost protection. Table 5 shows that the protected area and the noise of the three impellers were nearly the same. The developed impeller could cover a protected area of 300 m^2 and its noise was 54.1 dB.

Table 5 Other Performance of the impellers

	Fulta	Navec	The developed
Airflow velocity at a distance of 30 m /m·s^{-1}	1.3	0.7	0.9
Protected area/m^2	308	284	300
Noise level/dB	53.1	55.5	54.1

4 Conclusions

A new impeller for frost protection wind machines was designed based on reverse engineering and CFD simulation. And its airflow disturbance performance was compared with the commercial ones.

1) The characteristic parameters of cross-section shape, installation angle, sweep angle, hub ratio and blade number were determined as the optimization factors by rebuilding a base impeller via reverse engineering.

2) A hypothetical wind tunnel was established to conduct CFD simulation under different combinations of the parameters for investigation of the impeller's aerodynamic performance. Based on the simulation analysis, the optimal combination of impeller parameters was: blade cross-section of ϕ2400 mm, installation angle of 15°, sweep angle of 87°, hub ratio of 0.3 and blade number of 4.

3) Field test results show that the maximum airflow velocity of the developed impeller at 12 m in front of it was higher than that of the control. The developed impeller took on better stability of disturbed airflow. It could cover an effective area of 300 m^2 without swing. Therefore, the optimal impeller had a potential to the application of tea plantation frost protection.

Acknowledgements

The authors are grateful to the financial support by National High Technology Research and Development Program of China (2012AA10A508), Special Fund of Non-profit Scientific Research for Agriculture (201303012) and Priority Academic Program Development of Jiangsu Higher Education Institutions (2014-37).

[References]

[1] Gu L, Hanson P J, Mac Post W. The 2007 eastern US spring freeze: Increased cold damage in a warming world. Bio Science, 2008; 58(3): 253–262. doi: 10.1641/B580311.

[2] Atkinson C J, Brennan R M, Jones H G. Jones H G. Declining chilling and its impact on temperate perennial crops. Environmental and Experimental Botany, 2013; 91: 48–62. doi: 10.1016/j.envexpbot.2013.02.004.

[3] Jalili A, Jamzad Z, Thompson K, Araghi M K, Ashrafi S, Hasaninejad M, et al. Climate change, unpredictable cold waves and possible brakes on plant migration. Global Ecology and Biogeography, 2010; 19(5): 642–648. doi: 10.1111/j.1466-8238.2010.00553.x.

[4] Leuning R, Cremer K W. Leaf temperatures during radiation frost (Part I): Observations. Agricultural Forest Meteorology, 1988; 42(2): 121–133. doi: 10.1016/0168-1923(88)90072-X.

[5] Hacker J, Neuner G. Ice propagation in plants visualized at the tissue level by infrared differential thermal analysis (IDTA). Tree physiology, 2007; 27(12): 1661–1670. doi: 10.1093/treephys/27.12.1661.

[6] Bates E M, Lombard P B. Evaluation of temperature inversions and wind machine on frost protection in southern Oregon. Special Report 514, Agricultural Experiment Station, Oregon State University, 1978.

[7] Meehl G A, Tebaldi C, Nychka D. Change in frost days in simulations of twenty first century climate. Climate Dynamics, 2004; 23(5): 495–511. doi: 10.1007/s00382-004-0442-9.

[8] Blank S C, Venner R. Evaluating the cost-effectiveness of risk-reducing inputs: wind machines for citrus. Hort Technology, 1995; 5(2): 165–170.

[9] Ribeiro A C, De Melo-Abreu J P, Snyder R L. Apple orchard frost protection with wind machine operation. Agricultural Forest Meteorology, 2006; 141(2-4): 71–81. doi: 10.1016/ j.agrformet.2006.08.019.

[10] Battany M C. Vineyard frost protection with upward-blowing wind machines. Agricultural and forest meteorology, 2012; 157: 39–48. doi:10.1016/j.agrformet. 2012.01.009.

[11] Wu W Y, Hu Y G, Zhang H, Sun H W. An improved design on suction-exhaust duct for frost protection in tea fields. Paper number: 141907096rev, In: Proceedings of the ASABE Annual Meeting, Montreal, Quebec Canada, 2014. pp.3548–3555. doi: 10.13031/aim.20141907096.

[12] Brown P. Anti-frost fan: US Patent: 4753034, 1988-6-28.

[13] Stafford T P, Calif G. Fan blade for wind machines: US Patent: 4148594, 1979-04-10.

[14] Maximize the performance of your wind machine with Pure Customization. http://www.orchard-rite.com/wind-machines/head-tower. Accessed on [2014-01-04].

[15] Frost damage to your crop can occur in as little as 20-30 minutes. http://www.hfhauff.com/blades.php. Accessed on [2013-02-07]

[16] Wu W Y, Hu Y G, Lu H Y, Asante E A, Liu S Z. Airfoil optimization design for frost protection wind machines using Profili software. International Agricultural Engineering Journal, 2015; 24(3): 43–51.

[17] Yang S. Design and experiment of a biconvex-airfoil wind machine for tea frost protection. Master's dissertation. Zhenjiang: Jiangsu University. 2014.

[18] Hu Y G, Li P P, Dai Q L, Zhang X L, Tanaka K H, Cui G L. System design and experiment on elevated wind machine for tea frost protection. Transactions of the CSAM, 2007; 20(12): 97–99, 124. doi: 10.3969/j.issn.1000-1298.2007.12.024. (in Chinese with English abstract)

[19] Li W C, Ren G X, Fan G X, Tang Y, Tang X L. Research status of the development and application of tea anti-frost fan. China Tea Processing, 2014; 2: 34–37. doi: 10.15905/j.cnki.33-1157/ts.2014.02.012. (in Chinese with English abstract)

[20] Qian X Y, Ichikawa S Y, Ito N T. Optimal structure design of anti-frost fans: Vibration analysis of structure based on model. In: Proceedings of the 50th Conference of Japanese Society of Agricultural Machinery. Tokyo, Japan. 1992.

[21] Qian X Y, Ichikawa S Y, Ito N T. Optimal design of anti-frost fans: Stress property. In: Proceedings of the 50th Conference of Japanese Society of Agricultural Machinery. Tokyo, Japan. 1992.

[22] Hu Y G. Mechanism and control technology of late frost protection for tea plant (*Camellia sinensis* L.) through air disturbance. PhD dissertation. Zhenjiang: Jiangsu University. 2011.

[23] Chang Z Z. Axial flow fan and practical technology. Beijing: China Machine Press, 2005.

[24] Zhou J H, Yang C X. Parametric design and numerical simulation of CPU axial-flow fan with application. Acta Electronica Sinica, 2008; 36(8): 1526–1531. doi: 10.3321/j.issn:0372-2112.2008.08.010. (in Chinese with English abstract)

[25] Yi Z Q, Xi D K, Lu S L, Zhao X, Sun G. Numerical simulation and experimental research on the fan. Machinery Design & Manufacture, 2007; 10: 98–101. doi: 10.3969/j.issn.1001-3997.2007.10.042. (in Chinese with English abstract)

[26] Tian X D, Shi G R, Ruan X Y. Key issue of complex surface part in reverse engineering. Journal of Machine Design, 2000; 4(29): 1–5. (in Chinese with English abstract)

[27] Vanco M, Brunnett G. Direct segmentation of algebraic models for reverse engineering. New York: Springer, 2004.